Dynamic OCT simulator based on mathematical models of intratissue dynamics, image formation, and measurement noise

Yuanke Feng[1], Shumpei Fujimura[1], Yiheng Lim[1], Thitiya Seesan[1], Rion Morishita[1], Ibrahim Abd El-Sadek[1,2], Pradipta Mukherjee[1,3] and Yoshiaki Yasuno[1]

[1]*Computational Optics Group, University of Tsukuba, Japan,* [2]*Faculty of Science, Damietta University, Egypt,* [3]*Indian Institute of Technology, Delhi*

ABSTRACT

Dynamic optical coherence tomography (DOCT) provides label-free functional imaging that analyzes the temporal OCT signal variations caused by intracellular and intratissue motilities. This study developed a simulator using mathematical models to describe seven categories of motilities: active transport, passive transport, intracellular jiggling, dissociation of floaters, intracellular flow, cell migration, and macroscopic flow. These motilities were modeled using random ballistic motion, diffusion, mono-directional translation and their combinations.

The simulator generates OCT signals by considering two image formations: single-point OCT signal formation and 3D spatial OCT signal formation. It includes physically accurate noise models to account for shot noise, relative intensity noise (RIN), and non-optical noise. The study computed three types of DOCT contrasts: logarithmic intensity variance (LIV), OCT correlation decay speed (OCDS), and amplitude power spectrum (APS). The findings show that as the scatterer velocity increases, LIV increases and the high-intensity band of APS broadens, indicating sensitivity to motion. Meanwhile, OCDS reaches a peak at a specific velocity range, further highlighting the dependence on scatterer speed.

The simulation results indicate that these DOCT contrasts are sensitive to the motion characteristics of scatterers, especially under random ballistic motion. The fidelity of DOCT signals is preserved when the signal-to-noise ratio (SNR) exceeds 30 dB but degrades significantly for the SNR below 10 dB. This simulator enhances the understanding of the relationship between DOCT signals and various motilities, and it helps the interpretation of specific intracellular and intratissue dynamics.

Keywords: Dynamic optical coherence tomography, dynamic scattering, mathematical modeling, intracellular activities, wave optics simulation, speckle, numerical noise.

1. INTRODUCTION

Dynamic optical coherence tomography (DOCT) has become a valuable label-free technique for functional tissue imaging, suitable for various applications including *in vitro* tumor pheroids[1] and organoids[2], *ex vivo* animal tissues[3], and *in vivo* human skin[4]. DOCT captures temporal fluctuations in OCT signals, reflecting intracellular and intratissue activities. However, it primarily measures OCT signal variations rather than direct tissue dynamics, leaving the precise relationship between DOCT signals and cellular or tissue motility ambiguous.

In this study, we present a comprehensive DOCT signal simulator. This software framework integrates mathematical models that depict intracellular and intratissue activities, alongside models for generating sequential OCT series considering physical models of measurement noise. A set of DOCT contrasts can be computed and further analyzed from the temporal OCT signal. For mathematical modeling, we categorized intracellular and intratissue activities into seven distinct types and used various physical frameworks to model scatterer motion, providing a detailed understanding of the underlying processes.

To demonstrate its capabilities, we conducted numerical simulations replicating the temporal fluctuations in OCT signals due to scatterer motion. We computed three DOCT contrasts: logarithmic intensity variance (LIV), OCT correlation decay speed (OCDS), and amplitude power spectrum analysis (APS). Using the simulator, we analyzed the relationship between DOCT signal properties, scatterer motion, and measurement conditions.

2. THEORETICAL FRAMEWORK

2.1. Motion models

The intracellular and intratissue activities have been categorized into seven distinct types, as outlined in the second column of Table 1. These seven activities are subsequently represented using three mathematical models and their combinations.

Table 1: Summary of mathematical modeling of intracellular/intratissue activities and the scatterer motion models. where $\boldsymbol{r}_{j,i}$ represents the 3D location of j-th scatterer at time point t_i, $\langle\ \ \rangle_j$ is the average over all the scatterers, D is the diffusion coefficient, $\boldsymbol{v}$ and v represent the velocity and its amplitude (i.e., speed) of scatterers, $\boldsymbol{e}_j$ is the unit velocity vector in the direction of j-th scatterer.

Scatterers	Activities	Mathematical models		Motion parameters
		Static model		
Proteins	Active transport	Random ballistic model	$\boldsymbol{r}_{j,i+1} - \boldsymbol{r}_{j,i} = v\boldsymbol{e}_j(t_{i+1} - t_i)$	Velocity amplitude
	Passive transport			
	Dissociation of floaters			
	Intracellular fluid flow	Diffusion model	$\langle(\boldsymbol{r}_{j,i+1} - \boldsymbol{r}_{j,i})^2\rangle_j = 6D(t_{i+1} - t_i)$	Diffusion coefficient
	Macroscopic flow			
Organelles	Intracellular jiggling	Mono-direction translation	$\boldsymbol{r}_{j,i+1} - \boldsymbol{r}_{j,i} = \boldsymbol{v}(t_{i+1} - t_i)$	Velocity amplitude and direction
Cell	Cell migration			

The first model is a random ballistic model, where each scatterer exhibits linear motion with a uniform velocity amplitude, while their motion directions are randomly distributed among the scatterers.

The second model is a diffusion model, wherein the temporal displacements of the scatterers in each dimension follow a random walk, adhering to a zero-mean normal distribution.

The third model is a mono-directional translation, in which all scatterers move uniformly in a same direction and share the same velocity amplitude. The specifics of these models are detailed in Table 1 and its accompanying caption.

2.2. Generation of time-sequential OCT

Our simulator is equipped with two types of models (methods) to generate time-sequential OCT images as summarized in Table 2. The first one is single-point signal formation model, where the sample is represented by Tomita's dispersed scatterer model[5] and a complex OCT signal at a single point in an image is computed as the summation of phasor contributions from each scatter. By making the scatter move by the motion model in Section 2.1, a time-sequence of a single-point OCT signal is simulated.

Table 2: Methods of OCT signal generation. s is the complex OCT signal, j is the index of scatterers, B is the scattering potential distribution representing the sample structure, ϕ_j is the phase offset of the j-th scatterer, P_c is a complex point spread function, $\boldsymbol{x}$ and $\boldsymbol{x}'$ are the lateral positions on a sample and image, A_j is the amplitude reflectivity of the j-th scatterer, $\boldsymbol{r}_j$ is the 3D location of j-th scatterer, λ is the wavelength of the incident light, n is the relative refractive index of the medium, and $2nz_j$ represents the round-trip optical path length of reflected light.

	Single-point simulation	3D simulation
Model	$s(\boldsymbol{x}'; z_0') = \sum_{j=1}^{N} B(x_j, z_0) e^{i\phi_j} P_c(\boldsymbol{x}' - \boldsymbol{x}_j, z_0')$ [5]	$E_j(\boldsymbol{r}) = A_j \exp\left(i\frac{2\pi \cdot 2nz_j}{\lambda}\right)\delta(\boldsymbol{r} - \boldsymbol{r}_j)$ $s(\boldsymbol{r}) = E_j(\boldsymbol{r}) * \mathrm{PSF}(\boldsymbol{r})$
Advantages	Fast	Pixelized spatial accuracy
	Small data size	Spatial noise addition capability
Disadvantages	No spatial information	Slow simulation speed
	No spatial noise addition capability	Discrete space

The second is 3D spatial OCT simulator. In this model, a 3D field with multiple scatterers is numerically generated. By convolving the 3D filed with a 3D point spread function, the 3D complex OCT signal was generated. Again, by inducing motion in the scatterer and iterating the simulation process, a temporal sequence of 3D OCT signals is generated.

The first model is accurate and fast to compute but cannot recapitulate spatial information, while the second model can represent both spatial and temporal properly of OCT signal dynamic but slow to compute. We can select a suitable model based on the purpose of the simulation.

2.2. Noise model

The simulator is capable of producing physically accurate noise in the generated OCT signals based on the noise model proposed by Seesan *et al.*[6] This model replicates both lateral and axial spatial correlation properties of three types of noise: shot noise, relative intensity noise (RIN), and non-optical noise, as summarized in Table 3.

Table 3: List of noise types and its spatial correlation property that can be used in the simulator. The axial correlation distance depends on the power spectral shape of the light source $S(k)$.

Properties / Noise type	Lateral correlation distance	Axial correlation distance
Shot noise	Zero	$\mathcal{F}[\sqrt{S(k)}]$
RIN	Zero	$\mathcal{F}[S(k)]$
Non-optical noise	Zero	Zero

2.3. DOCT algorithms

We calculated three types of DOCT signals from the simulated OCT time-sequence using this simulator. The first is the logarithmic intensity variance (LIV), which is the time variance of the dB-scaled OCT intensity signals[7]. The second is OCT correlation decay speed (OCDS), which is the temporal decorrelation rate (speed) of OCT intensity signal[7]. It should be noted that the OCDS has one free parameter, the range of the decorrelation curve used to determine the decoration rate, and it can be freely selected in the simulation. The third is the amplitude power spectrum (APS)[8], which is the amplitude of the temporal Fourier transformed spectrum of the OCT signal amplitude.

2. DOCT ANALYSIS EXAMPLES

As examples of DOCT simulation, we studied the relation between three DOCT contrasts (i.e., LIV, OCDS and APS) and the scatterer velocity considering random ballistic model. Additionally, we calculated the signal-to-noise dependency of these DOCT signals by numerically adding the non-optical noise.

4.1. Simulation protocol

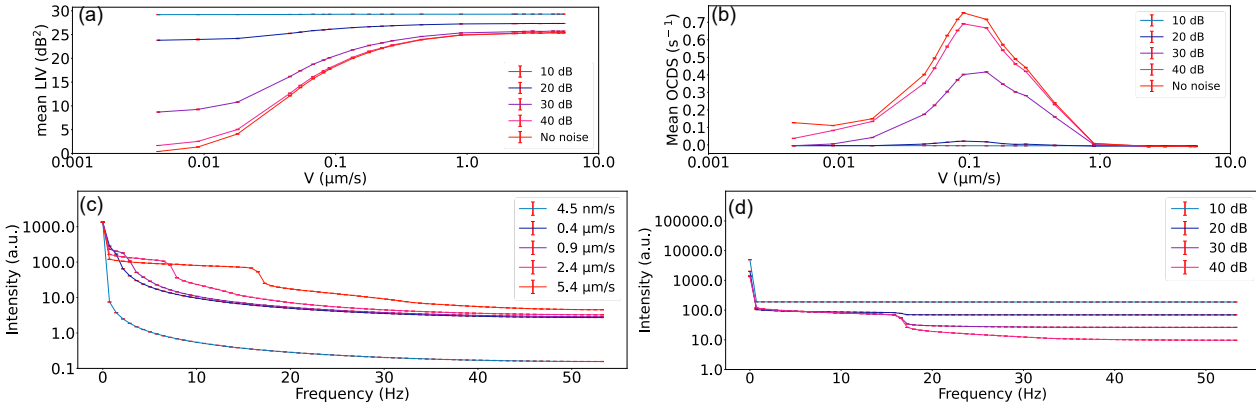

Figure 1: LIV (a), OCDS (b), APS without noise (c) versus scatterer velocity and APS with noise (d) versus SNR considering random ballistic model.

Two scanning protocols were evaluated. The first protocol involves a 32-frame sequence scan with a long inter-frame interval. The total acquisition time is 6.35 s, and the inter-frame interval is 204.8 ms. This 32-frame protocol was employed for LIV and OCDS computation.

The second protocol consists of acquiring 150 sequential frames with a short inter-frame interval. The total acquisition time is 1.39 s, and the inter-frame interval is 9.33 ms. This protocol was used for power spectra analysis.

The probe wavelength of the OCT system is 1310 nm, with resolutions of 14 μm axially and 18 μm laterally. The OCT system operates with non-optical noise, meaning the noise is spatially independent. The scatterer speed is set as [4.5 nm/s, 5.4 μm/s]. The set signal-to-noise ratio ranges from 0 to 40 dB.

4.2. Simulation result

Figure 1 (a-c) depicts the mean LIV, OCDS, and APS at varying velocity amplitudes. Each data point represents the average of 8 simulation trials, with error bars indicating the standard deviation. In Figure 1(a), LIV increases with velocity until it plateaus. The high-intensity band (except the DC component) of the power spectrum broadens with increasing velocity, highlighting sensitivity to scatterer speed [Figure 1(c)]. OCDS exhibits a peak at a specific velocity [Figure 1(b)], which is likely associated with the decorrelation delay range used to determine the decorrelation rate, which in this case is

[204.8, 1228.8 ms]. Our simulator can identify the relationship between peak velocity and delay range, making the OCDS interpretable in terms of intratissue activities.

Figures 1(a), (b), and (d) illustrate the mean LIV, OCDS, and APS (full spectral shape) for scatterers undergoing random ballistic motion at various SNRs. All three DOCT signals show sensitivity to velocity when the SNR exceeds 30 dB. However, when the SNR drops below 10 dB, the DOCT signals cease to respond to scatterer motion. This simulation provides insight into the reliability of DOCT measurements under different SNR conditions.

CONCLUSION

In this study, we developed a DOCT signal simulator that correlates intratissue and intracellular motilities with DOCT signals. This software framework integrates mathematical models that depict intracellular and intratissue activities, alongside models for generating sequential OCT series and physical models of measurement noise. We categorized these activities into seven distinct types and used various physical frameworks to model scatterer motion. As demonstration examples of this simulator, we studied the relation between three DOCT contrasts and the scatterer velocity considering random ballistic model and investigated their SNR dependency. Under the specific conditions of this simulation, DOCT values are found to be reliable when the SNR exceeds 30 dB.

REFERENCES

[1] El-Sadek, I. A., Miyazawa, A., Shen, L. T.-W., Makita, S., Mukherjee, P., Lichtenegger, A., Matsusaka, S. and Yasuno, Y., "Three-dimensional dynamics optical coherence tomography for tumor spheroid evaluation," Biomed. Opt. Express **12**(11), 6844–6863 (2021).

[2] Morishita, R., Suzuki, T., Mukherjee, P., El-Sadek, I. A., Lim, Y., Lichtenegger, A., Makita, S., Tomita, K., Yamamoto, Y., Nagamoto, T. and Yasuno, Y., "Label-free intratissue activity imaging of alveolar organoids with dynamic optical coherence tomography," Biomed. Opt. Express **14**(5), 2333–2351 (2023).

[3] Mukherjee, P., Miyazawa, A., Fukuda, S., Yamashita, T., Lukmanto, D., Okada, K., El-Sadek, I. A., Zhu, L., Makita, S., Oshika, T. and Yasuno, Y., "Label-free functional and structural imaging of liver microvascular complex in mice by Jones matrix optical coherence tomography," 1, Sci. Rep. **11**(1), 20054 (2021).

[4] Guo, Y., Morishita, R., El-Sadek, I. A., Mukherjee, P., Zhu, Y. and Yasuno, Y., "In vivo dynamic optical coherence tomography with hardware- and software-based motion correction," Opt. Coherence Tomogr. Coherence Domain Opt. Methods Biomed. XXVIII **12830**, 158–161, SPIE (2024).

[5] Tomita, K., Makita, S., Fukutake, N., Morishita, R., El-Sadek, I. A., Mukherjee, P., Lichtenegger, A., Tamaoki, J., Bian, L., Kobayashi, M., Mori, T., Matsusaka, S. and Yasuno, Y., "Theoretical model for en face optical coherence tomography imaging and its application to volumetric differential contrast imaging," Biomed. Opt. Express **14**(7), 3100–3124 (2023).

[6] Seesan, T., Mukherjee, P., El-Sadek, I. A., Lim, Y., Zhu, L., Makita, S. and Yasuno, Y., "Optical-coherence-tomography-based deep-learning scatterer-density estimator using physically accurate noise model," Biomed. Opt. Express **15**(5), 2832–2848 (2024).

[7] El-Sadek, I. A., Miyazawa, A., Shen, L. T.-W., Makita, S., Mukherjee, P., Lichtenegger, A., Matsusaka, S. and Yasuno, Y., "Three-dimensional dynamics optical coherence tomography for tumor spheroid evaluation," Biomed. Opt. Express **12**(11), 6844–6863 (2021).

[8] Münter, M., Pieper, M., Kohlfaerber, T., Bodenstorfer, E., Ahrens, M., Winter, C., Huber, R., König, P., Hüttmann, G. and Schulz-Hildebrandt, H., "Microscopic optical coherence tomography (mOCT) at 600 kHz for 4D volumetric imaging and dynamic contrast," Biomed. Opt. Express **12**(10), 6024–6039 (2021).